

---

# MULTI-RESOLUTION LARGE-EDDY SIMULATION OF AN ARRAY OF HYDROKINETIC TURBINES IN A FIELD-SCALE RIVER: THE ROOSEVELT ISLAND TIDAL ENERGY PROJECT IN NEW YORK CITY

---

A PREPRINT

**Saurabh Chawdhary**

Mathematics and Computer Science Division,  
Argonne National Laboratory,  
Argonne, Illinois 60439, USA.  
sauc@anl.gov

**Dionysios Angelidis**

Department of Civil Engineering  
College of Engineering and Applied Sciences  
Stony Brook University, Stony Brook, New York 11794, USA.

**Jonathan Colby & Dean Corren**

Verdant Power Inc.  
The Octagon, 888 Main Street  
New York, NY 10044, USA.

**Lian Shen**

St. Anthony Falls Laboratory  
Department of Mechanical Engineering  
University of Minnesota  
2 Third Ave SE, Minneapolis, MN 55414, USA.

**Fotis Sotiropoulos**

Department of Civil Engineering  
College of Engineering and Applied Sciences  
Stony Brook University, Stony Brook, New York 11794, USA.  
fotis.sotiropoulos@stonybrook.edu

October 9, 2018

## ABSTRACT

Marine hydrokinetic (MHK) power generation systems enable harvesting energy from waterways without the need for water impoundment. A major research challenge for numerical simulations of field-scale MHK farms stems from the large disparity in scales between the size of waterway and the energy harvesting device. We propose a large-eddy simulation (LES) framework to perform high-fidelity, multi-resolution simulations of MHK arrays in a real-life marine environment using a novel unstructured Cartesian flow solver coupled with a sharp-interface immersed boundary method. The potential of the method as a powerful engineering design tool is demonstrated by applying it to simulate a 30 turbine MHK array under development in the East River in New York City. A virtual model of the MHK power-plant is reconstructed from high-resolution bathymetry measurements in the East River and the 30 turbines placed in 10 TriFrame arrangements as designed by Verdant Power. A locally refined, near the individual turbines, background unstructured Cartesian grid enables LES across a range of geometric scales of relevance spanning approximately five orders of magnitude. The simulated flow-field is compared with a baseline LES of the flow in the East River without turbines. While velocity deficits and increased levels of turbulence kinetic energy are observed in the vicinity of the turbine wakes, away from the turbines as well as on the water surface only small increase in mean momentum is found. Therefore, our results point to the conclusion that MHK energy harvesting from large rivers is possible without a significant disruption of the river flow.

**Keywords** East River · marine and hydrokinetic · MHK · local refinement · unstructured Cartesian grids · LES · tidal · energy · turbine

## 1 Introduction

While hydropower has been the major resource for generating electricity from water, marine and hydrokinetic (MHK) systems can harness energy from flowing natural streams of water without needing dams for impounding water (Khan et al., 2009). Instead, they make use of MHK devices to extract energy from rivers, tidal channels, and ocean currents. Axial hydrokinetic turbines are a popular choice of device to extract MHK energy and have been deployed in the field (Torrens-Spence et al., 2017; Williamson et al., 2016; OpenEI, 2008) as well as studied analytically, experimentally and computationally (Nishino and Willden, 2012b; Batten et al., 2008; Gant and Stallard, 2008; Kang et al., 2012, 2014; Malki et al., 2014; Chawdhary et al., 2017; Angeloudis et al., 2018).

Despite the recent advances in numerical methods and the exponential growth of computing power, numerical study of MHK turbine arrays at field-scale rivers remains a major challenge. Marine environments are dominated by complex bathymetry and a wide range of natural and man-made structures that give rise to turbulent flows dominated by energetic, large-scale coherent structures. Introducing MHK devices in such a complex fluid flow environment gives rise to additional complexities in the turbulent flow due to turbine-turbine and turbine-bathymetry interactions, which give rise to flow phenomena spanning a broad range of temporal and spatial scales. Such phenomena need to be understood and quantified in order to optimize MHK arrays for energy extraction and evaluate the structural integrity and reliability of the devices in the harsh waterway fluvial environment (Li et al., 2011; Kang and Sotiropoulos, 2012; Tatum et al., 2016; Musa et al., 2018). Computational modeling presents the only viable approach for gaining such understanding at field scale and on a site-specific basis.

Computational tools capable of tackling such complex flows, however, need to be able to resolve waterway and device induced turbulence, which occurs at high Reynolds numbers, across a range of scales, and is dominated by inherently 3D energetic coherent structures. For the most part, field-scale simulations of large rivers have been performed using two-dimensional (2D) models by solving the shallow-water equations (Abderrezzak et al., 2009; Casulli and Walters, 2000; Heniche et al., 2000; Yoon and Kang, 2004; Lee et al., 2017) or statistically stationary 3D models based on the Reynolds-averaged Navier-Stokes (RANS) equations (Ge and Sotiropoulos, 2005; Nagata et al., 2005; Lu and Wang, 2009; Baranya et al., 2015), due to their simplicity and computational expedience. Computational methods for carrying out eddy-resolving simulations in real-life rivers have only recently began to appear in the literature (Kang and Sotiropoulos, 2015; Khosronejad et al., 2016b,a; Wilcox et al., 2017). Such models, however, have yet to tackle the simulation of MHK devices in real-life river environments.

James et al. (2010) used a modification of the Environmental Fluid Dynamics Code (EFDC) (Hamrick, 2007) developed at Sandia National Laboratories (SNL) to simulate changes in the marine environment caused by an array of MHK turbines, by modeling MHK turbines as single energy extraction points in a 2D domain. Other previous studies have used unsteady Reynolds-Averaged Navier Stokes (RANS) modeling to simulate flows in idealized channel geometries with actuator disc model to model the turbines, but without accounting for the prevailing features of the surrounding marine environment (Bai et al., 2009; Abolghasemi et al., 2016). LES has been widely applied as a powerful computational tool in the highly relevant field of wind farm optimization (Churchfield et al., 2012; Yang et al., 2013b; Porté-Agel et al., 2013; Vasel-Be-Hagh and Archer, 2017; Yang et al., 2018). Conclusions from such studies, however, are of limited use for MHK energy systems due to inherent differences between the ambient atmospheric flow in wind farms (e.g. the size of the wind turbine relative to the thickness of the atmospheric boundary layer) and the fully developed turbulence in waterways (where the MHK turbines occupy a considerable part of the flow depth) (Chamorro et al., 2013). Churchfield et al. (2013) are developing a framework for simulating MHK turbine arrays in natural waterways (Churchfield et al., 2013) and have applied it to study the effects of turbulence in the incoming flow on the wake characteristics in an artificial straight channel using LES and actuator disk parameterization. Wilcox et al. (2017) performed site-specific detached-eddy simulation (DES) of turbulent flow in the Fundy Tidal Region at field scale to gain insight about the placement of tidal turbines. However, the simulations with turbines was planned for future work.

Sotiropoulos and co-workers have recently developed an advanced computational fluid dynamics framework, the Virtual Flow Simulator (VFS-Rivers), capable of carrying out site-specific LES in real-life waterways with stationary and/or mobile river beds (Sotiropoulos, 2015). VFS-Rivers employs the curvilinear immersed boundary (CURVIB) method (Ge and Sotiropoulos, 2007a; Kang et al., 2011) with wall models for carrying out LES in arbitrarily complex domains with arbitrarily complex immersed boundaries and migrating bedforms. The predictive capabilities of VFS-Rivers have been extensively demonstrated for flows in man-made field scale streams Kang et al. (2011), natural streams (Khosronejad et al., 2016a), and large rivers under baseline and extreme flooding conditions Khosronejad et al. (2016b). VFS-Rivers has also been applied to carry out high-fidelity LES of a single MHK turbine (Kang et al., 2012, 2014) and MHK turbines in a TriFrame arrangement (Chawdhary et al., 2017) in a laboratory straight open channel. In all cases, excellent agreement with laboratory and field-scale (where available) measurements have been reported and the ability of the code to uncover new physics that could not be accessed by experiments alone has been demonstrated (see for example Kang et al. (2014)).

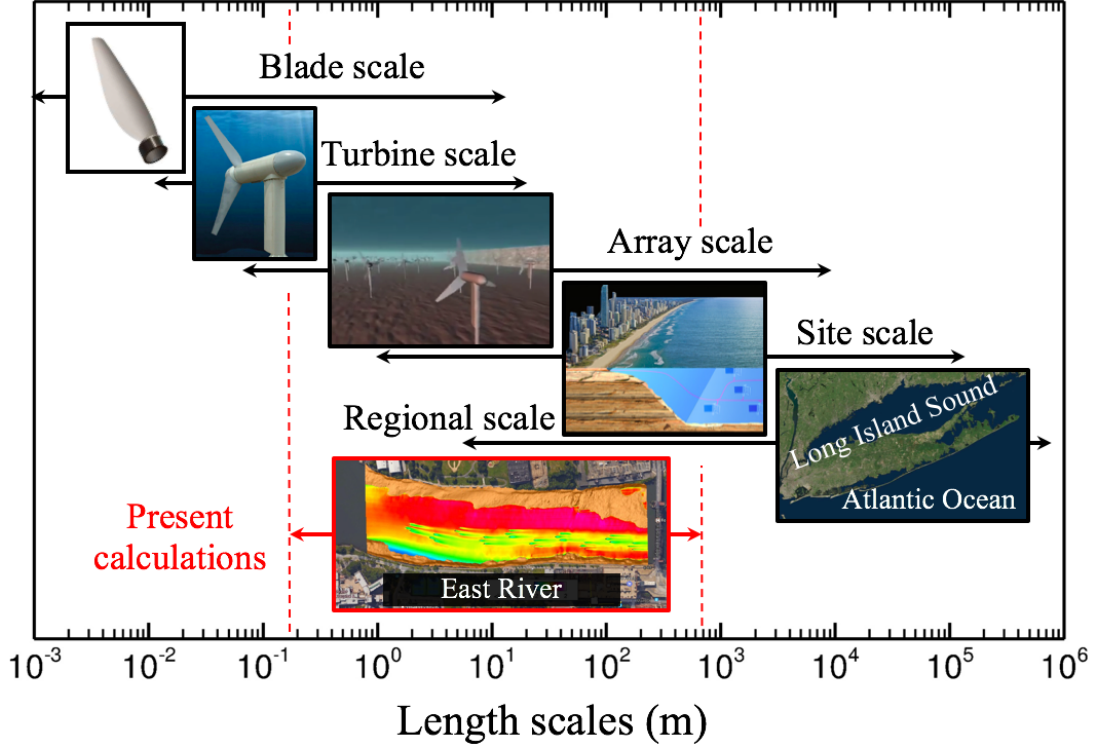


Figure 1: Schematic showing the range of length scales present in hydrodynamic modeling of MHC energy systems at different physical dimensions involved. (Adapted from Adcock et al. (2015)). The simulation in this paper resolves flow scales across multiple ranges, as marked in red.

In spite of the aforementioned recent progress, high-fidelity computational methods that can carry out LES of MHC turbines and multi-turbine arrays in real-life waterways, resolving waterway and device-induced unsteady coherent structures, have yet to be proposed in the literature. The reason for this is illustrated in Fig. 1, which describes the various length scales present in the flow when a turbine is placed in a natural marine environment like a tidal channel. The blades of the turbine can be very thin giving rise to small scale flow structures (of the order of centimeters) whereas the turbine diameter itself is normally of the order of few meters. A multi-turbine array introduces flow scales which, depending on the array configuration, can be beyond an order of magnitude larger than the turbine diameter. Furthermore, when modeling a particular array installation site or a larger marine environment, the flow characteristics of the region (river and/or ocean system) also come into play as they determine the ambient and inflow conditions to the turbine array. As recent as few years ago, Stoesser et al. (2010) noted that “because of the high computational cost, LES can currently only be used for lower Reynolds numbers making it not directly applicable in the river engineering practice where usually Reynolds numbers are above  $10^6$  and computational domains sizes range from several hundred meters to kilometers”. Other researchers have also acknowledged the computational challenges in dealing with natural geometries (Abad et al., 2008; Kang and Sotiropoulos, 2012). Kang et al. (2012, 2014); Gant and Stallard (2008); Batten et al. (2008); Malki et al. (2014) and Chawdhary et al. (2017) have studied flow past turbines using LES to resolve scales in one or two of the scale ranges shown in Fig. 1.

In this work we seek to demonstrate for the first time that LES of multi-turbine MHC farms in real-life waterways resolving coherent structures spanning the scales of the river to the scale of the turbine rotor and wake are now well within reach. For that, we implement a recently developed numerical method capable of local mesh refinement on unstructured Cartesian grids (Angelidis et al., 2016) in the new version of the VFS-Rivers code to enable multi-resolution simulations of MHC arrays in a real-life waterway. The specific case we consider herein is the Roosevelt Island Tidal Energy (RITE) project currently under development in the East River in New York City by Verdant Power. We employ high-resolution bathymetry measurements and the turbine layout proposed by Verdant Power to reconstruct a virtual model of the East River tidal power plant. The resulting digital model of the East River power plant is embedded in a background Cartesian mesh locally refined in the vicinity of the turbines to carry out LES at field scale using the method developed by Angelidis et al. (2016). Our work makes a number of novel contributions to the literature by: a) Demonstrating the potential of the geometry-based adaptive mesh refinement methodology in performing

high-fidelity, multi-resolution LES for real life aquatic environments; b) Bridging computationally for the first time the large disparity of scales between the coherent structures induced by the energy harvesting device and those induced by the waterway within which the devices are embedded in so that turbine-turbine and turbine-waterway interactions can be studied numerically at field scale and c) illustrating the utility of site-specific LES as a powerful tool for enabling simulation-based optimization of MHK powerplants at field scale.

This paper is organized as follows. In section 2, we briefly discuss the numerical method used for the simulations. In section 3, we validate the numerical method by simulating a model wind farm and comparing simulations with measurements. Section 4 describes the deployment site of the hydrokinetic turbine array simulated herein. Section 5 presents results from baseline simulations of the relevant reach of the East River without the turbine array. Section 6 presents simulation results for the 30 turbine array installed in the East River and discusses its effects on the river flowfield. Finally, in section 7 we summarize the findings of this work and discuss future directions.

## 2 Numerical Methods

The new version of VFS-Rivers, incorporating the unstructured Cartesian flow solver of Angelidis et al. (2016), is employed herein to perform multi-resolution LES past the RITE turbine array. The equations governing the instantaneous, resolved flow field for three-dimensional, incompressible, turbulent flow are the spatially-filtered continuity and Navier-Stokes equations employed in LES models. The sub-grid scale (SGS) stress tensor representing the effects of the SGS motions on the resolved fields of the LES is modeled using the Smagorinsky model (Smagorinsky, 1963). The governing equations are discretized on a 3D hybrid staggered/non-staggered grid layout (Ge and Sotiropoulos, 2007b) adapted on unstructured Cartesian grids using the second-order central differencing scheme when stencil cells are at same level of refinement. When computational cells are surrounded by other cells of varying level of refinement, hanging nodes and a bi-quadratic operator are utilized to facilitate the spatial discretization using a hybrid second-order upwind scheme. Time integration of governing equations is performed using the fractional step algorithm such that the discrete divergence of the velocity field is satisfied to machine zero at every time step. The implicit solution of the momentum equation is achieved by using a Jacobian-free Newton-Krylov method coupled with the generalized minimal residual solver (GMRES) of Saad and Schultz (1986). The unstructured flow solver is efficiently parallelized using the portable, extensible toolkit for scientific computation (PETSc) libraries and message passing interface (MPI) (Balay et al., 1997, 2014, 2016). The PETSc libraries are also used to solve the momentum equation using the aforementioned Jacobian-free Newton-Krylov method. The high performance preconditioners (HYPRE) libraries (Falgout et al., 2006) with BoomerAMG (Yang and Henson, 2002) preconditioner are used for solving the Poisson equation. We use the actuator line model for modeling the axial turbines in the flow where the blades of turbines are represented using rotating line forces in the flow (Angelidis et al., 2016; Yang et al., 2015). The sharp interface immersed boundary method approach in VFS-Rivers is employed to simulate arbitrarily complex immersed boundary in the flow domain – the river bathymetry in this case. In this method, the immersed irregular structures are represented using unstructured triangulated surface meshes embedded within a locally refined Cartesian background grid. The effect of immersed boundaries on the flow (i.e. the river bathymetry in this case) is accounted for by reconstructing at every time step boundary conditions at the nodes in the immediate vicinity of the boundary via interpolation along the local normal to the boundary direction. Given the high Reynolds number of the flows of interest, the interpolation to reconstruct velocity boundary conditions is implemented using a wall model (see Yang et al. (2012) for details). The freesurface boundary of the flow channel is treated as a rigid lid, an assumption which has been successfully applied in the previous works of Kang et al. (2011, 2012, 2014) and Yang et al. (2013a) among others, for low Froude number flows ( $Fr \approx 0.2$  for the flow in the East River). More details about numerical method can be found in Angelidis et al. (2016).

## 3 Model validation : Flow over aligned wind turbine array

In Angelidis et al. (2016) we validated the unstructured Cartesian flow solver for several cases including turbulent flows over stand-alone wind and hydrokinetic turbines. In this section we seek to demonstrate the predictive ability of the solver in LES of turbine arrays. Since no data is available for MHK arrays, we employ herein the results of a well documented wind tunnel experiment for a model wind farm.

### 3.1 Test case and computational details

We carry out LES of turbulent flow past a  $6 \times 3$  aligned array of model wind turbines spaced  $5D$  and  $4D$  apart of each other in the streamwise ( $z$ ) and spanwise ( $x$ ) directions, respectively. Each model wind turbine has diameter  $D = 0.15m$  and hub height  $h = 5D/6$ . The tip-speed ratio (TSR),  $\lambda$ , for all the turbines is  $\lambda = 4.1$  and the Reynolds number,  $Re$ , based on the rotor diameter,  $D$ , and the mean incoming hub height velocity,  $W_h$ , is  $Re = 2.5 \times 10^4$ . Details of the

corresponding wind tunnel experiment can be found in the work of Chamorro and Porte-Agel (2011). We note that the same test case has also been investigated numerically by Yang et al. (2013b) using the Virtual Flow Simulator (VFS) (Calderer et al., 2015) to carry out LES on a structured Cartesian grid without refinement.

The computational domain extends  $12D$ ,  $5D$  and  $33D$  in the spanwise ( $x$ ), vertical ( $y$ ) and streamwise ( $z$ ) directions, respectively. Two simulations are carried out, the first is performed on a uniform structured Cartesian grid (G1) with  $N_x=121$ ,  $N_y=61$  and  $N_z=331$  gridnodes in  $x$ ,  $y$  and  $z$  directions, respectively, and the second is performed on a locally refined mesh (G2) which is generated after remeshing the primary structured Cartesian grid (G1) in a cylindrical manner around the mid-column rotors, by applying up to two levels of refinement. Thus, G1 consists of  $2.4 \times 10^6$  cells, and the resulting grid spacing around all the turbine rotors is  $D/10$ ,  $D/12$  and  $D/10$  in  $x$ ,  $y$  and  $z$  directions, respectively. To generate the unstructured grid G2, we apply two levels of refinement around the mid-column wind turbines in a cylindrical manner and the center of the finite cylinders is located at the turbines' hub height. The first level of refinement is located within a cylindrical region with a radius of  $R_{ref1} = 0.7D$  which extends between  $0.8D \leq z \leq 32D$  from the inlet and the second level of refinement is applied within six cylindrical zones with a radius of  $R_{ref2} = 0.6D$  and length of  $L_{ref2} = 2D$  located symmetrically around the turbine rotors. The equivalent uniform structured Cartesian grid having the resolution same as that around the turbine rotors, would consist of  $1.5 \times 10^8$  computational cells. The resolution around the turbine rotors of the middle column in G2 is equivalent to the finest spatial discretization used in the work of Yang et al. (2013b) using a stretched Cartesian structured grid with  $17.3 \times 10^6$  cells. To generate inflow conditions, we carry out LES for a domain of the same cross-section as the computational domain with the turbines but without the turbines and with periodic conditions applied in the streamwise direction. This simulation is continued until statistical convergence is achieved. Instantaneous flowfields from the statistically stationary flowfields are stored and subsequently used to prescribe instantaneous boundary conditions at the inlet of the wind farm domain. Free slip conditions are applied at the top and spanwise boundaries and the wall model of Wang and Moin (2002) is used as boundary condition on the bottom boundary. The turbines are parameterized using the actuator line model as described in Yang et al. (2015). The time step is equal to  $\tau = 0.001D/W_h$ . The simulations are first run for 25 revolutions of the turbines until the total kinetic energy of the domain reaches a quasi-steady state. Subsequently, the results are time averaged for another 55 rotor revolutions to compute the statistics presented below.

### 3.2 Comparison with experimental measurements and numerical data

Streamwise profiles of the calculated (with and without refinement) time-averaged streamwise velocity ( $W$ ) are compared with the measurements of Chamorro and Porte-Agel (2011) and the LES of Yang et al. (2013b) at different vertical locations on a  $x$ - $z$  plane passing through the center of the middle column wind turbines in Fig. 2. At the bottom tip of the wind turbines (Fig. 2(a)), the present calculations agree well with the experimental measurements with a small over-prediction of the time-averaged streamwise velocity observed in the wake of the first and second wind turbines. Our results are in very good agreement with the experimental measurements in the wake of the fourth, fifth and sixth wind turbines where the calculations of Yang et al. (2013b) slightly under-predict the streamwise velocity. Overall the calculations performed on a 2-level locally refined grid agree very well with the experimental measurements. It is seen in Fig. 2(b) that the calculations performed on a locally refined grid, G2, result in better prediction of the near-wake time-averaged streamwise velocity compared to calculations performed on the primary grid G1 and calculations on stretched Cartesian grids (Yang et al., 2013b). At the top tip of the wind turbines (Fig. 2(c)), small discrepancies are observed mostly in the wake of the first wind turbine; however, very good agreement is obtained for all the other locations. The maximum discrepancy found 1D downstream of the first turbine is approximately 10%. The maximum discrepancy in the wake of the rest of the turbines at hub height is less than 5% (at a location approximately 1D downstream of the second turbine).

Figure 3 shows contours of the mean velocity and turbulence statistics along the vertical plane passing through the center of the wind farm. In line with the observations of Yang et al. (2013b), the velocity deficit in the wake of the first wind turbine is much weaker compared to the wakes of the other turbines which are nearly the same (Fig. 3(a)). The actuator line model can also predict the significant levels of time-averaged spanwise velocity induced by the rotating turbines; which is more intense in the wake of the first and second turbines (Fig. 3(b)). The distribution of the time-averaged velocity profiles provides evidence of the smooth transition of the flow properties across cells with different levels of refinement (Angelidis et al., 2016). Figure 3(c) depicts contours of the streamwise turbulence intensity computed on a 2-level refined grid. The velocity fluctuations in the wake and at the top tip of the wind turbines result in the formation of a layer of enhanced turbulence intensity, which transitions to higher levels with downwind distance. The turbulence intensity is larger at the top tip compared to the bottom tip shear layer as a result of the interaction of the turbine wakes with the wall boundary layer. We may also observe the development of a region with significant turbulence intensity just behind the turbines at the hub height. Figure 3(d) shows the contour plots of Reynolds shear stress,  $-\langle v'w' \rangle$ , normalized by the incoming hub height velocity,  $W_h$ . The turbines introduce positive kinematic shear stress in the wakes at the top-tip and negative stress below the turbine hub height, respectively. The absolute kinematic shear stress

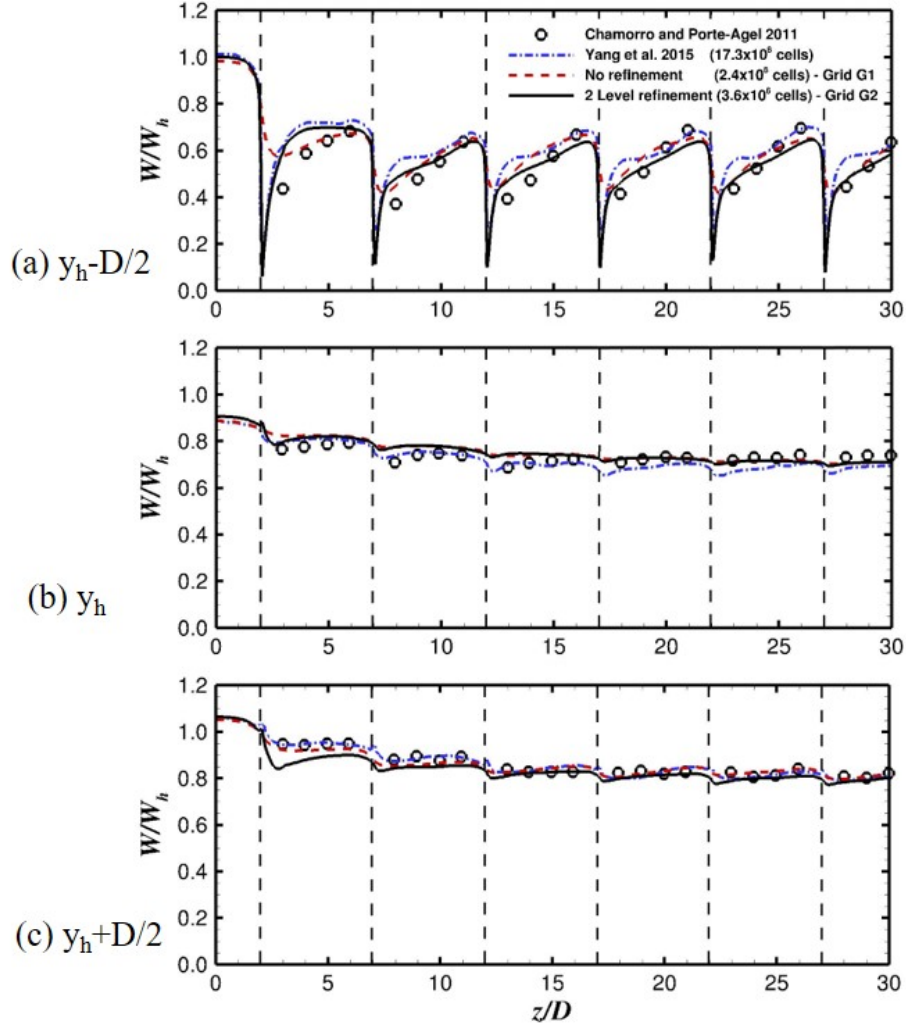


Figure 2: Comparison of the mean streamwise wind velocity at different vertical locations, along the streamwise direction, on a  $x$ - $z$  plane passing through the center of the middle column wind turbines. Calculations performed on a uniform Cartesian grid  $121 \times 61 \times 331$  without refinement (G1) and on a 2-level refined grid adapted around and in the wake of the wind turbines' rotor (G2). Comparison is performed against previous experimental measurements of Chamorro and Porte-Agel (2011) and numerical simulations of Yang et al. (2013b).

at the top tip height is significantly larger compared to the values in lower regions, indicating that the high levels of vertical flux of streamwise momentum are associated with the intense shear layer. Overall, the results presented in this section show that our calculations are in good agreement with the experimental measurements of Chamorro and Porte-Agel (2011). The discretization of the governing equations on a locally refined unstructured Cartesian grid enabled achievement of comparable level of accuracy with the calculations of Yang et al. (2013b) while using 5 times smaller number of computational cells.

#### 4 The East River site and computational setup

The East River is a tidal strait in New York City that connects New York Harbor and the Atlantic Ocean to Long Island Sound. An aerial view of New York City in Fig. 4(a) shows its location between Manhattan and Queens. The present study is part of the RITE Project, a pilot project which aims to install up to one Megawatt of MHK power in the East Channel of the East River. The Federal Energy Regulatory Commission (FERC) has issued a commercial pilot license (#P-12611) to *Verdant Power*. The region where MHK turbine array is proposed to be installed is indicated in Fig. 4(c). The East River being a tidal strait starts and ends in ocean and the flow is driven by the difference in tidal heights with a

semi-diurnal time period of about 12 hours. In spite of the varying nature of the flow, it is possible to treat the flow as unidirectional for the purpose of our study for the following reasons: (1) the time scale (12 hours) of flow pulsation is much larger than the time taken for the hydrodynamics within the simulated section to attain a statistically converged steady state – the simulations were run for a total physical time of 900 s; and (2) the turbines in the flow are allowed to yaw so that they are approximately aligned with the primary flow direction. The tidal channel bed is a cobble layer of rocks larger than the size that can be mobilized by the flow eliminating the need for sediment transport modeling.

#### 4.1 Deployment of the Triframes in East River

The map in Fig. 4(c) shows the FERC licensed boundary within which the turbines are to be installed. Verdant Power has developed Kinetic Hydro-Power System (KHPS) turbines that will be used to harvest kinetic energy from the channel. These are 3-blade axial turbines 5 m in diameter. The power generation capacity of these machines, which naturally varies with time as a function of the instantaneous water flow velocity, is 56 kW and their rated power in the RITE site flow velocity distribution is 35 kW (Verdant Power, 2010). Verdant Power has successfully performed deployment of individual turbines at the site. The proposed plan is to deploy up to 30 turbines in the East Channel of the East River in several phases with constant testing and environmental monitoring. For structural reasons and

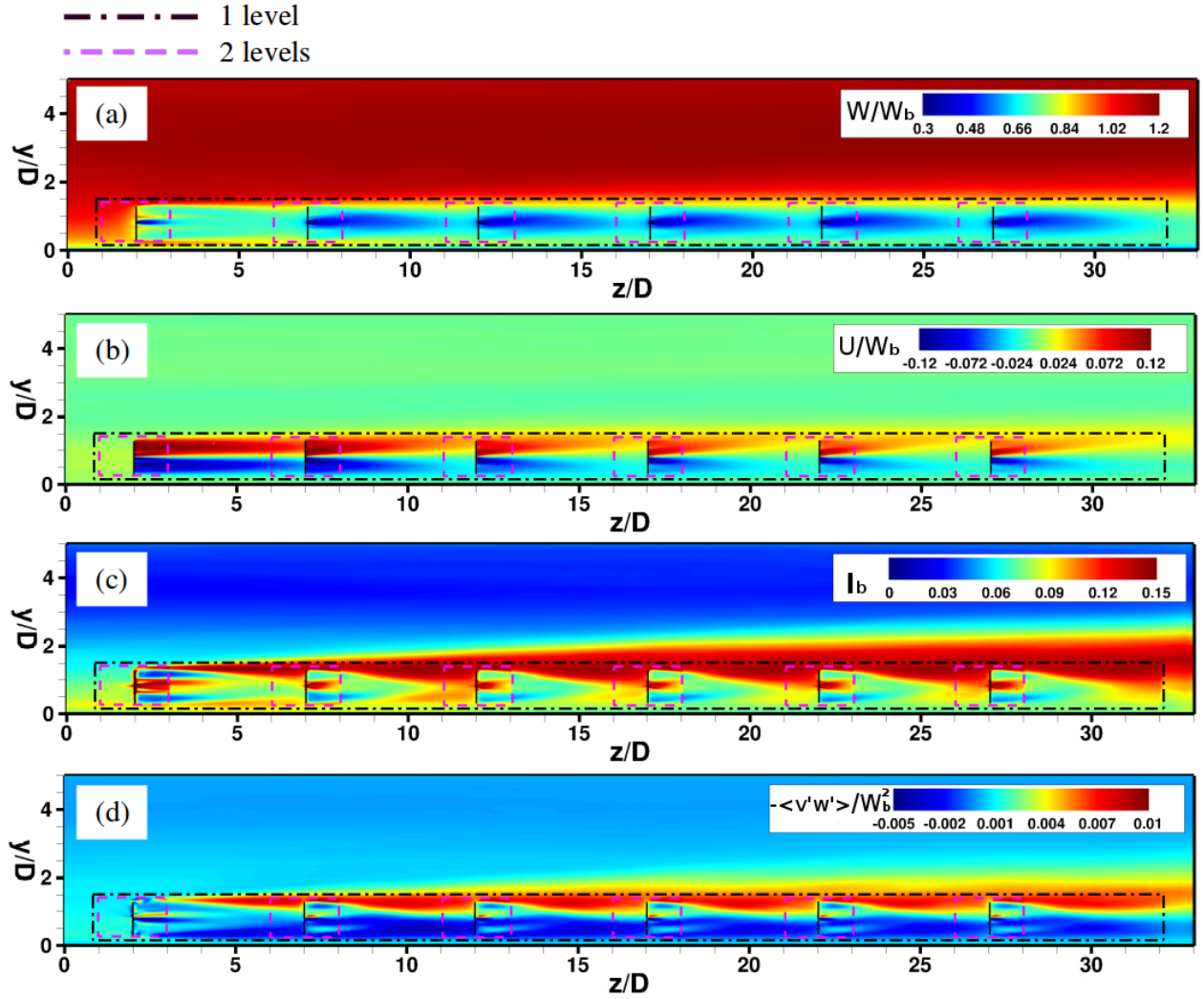


Figure 3: Contours of the time-averaged: (a) streamwise wind velocity; (b) spanwise wind velocity; (c) streamwise turbulence intensity; (d) Reynolds shear stress, on a  $y$ - $z$  plane passing through the center of the wind turbines located in the middle column. The plotted values are normalized by the incoming hub height velocity,  $W_h$ , and the calculations are performed on a 2-level refined grid consisted of  $3.6 \times 10^6$  computational cells.

ease of deployment the turbines are to be installed on the river bed in 10 TriFrame arrangements – i.e. sets of three turbines mounted on the apexes of a common triangular base. The proposed locations of the TriFrames are marked in Fig. 4(c) by triangles. Underwater cables from each unit connect to the onshore controls and the electric grid. The estimated average annual production from the array is between 1680 – 2400 *MWh* (Verdant Power, 2010). The electricity produced will be added to the grid and used to power buildings in Roosevelt Island.

#### 4.2 Construction of the digital terrain model

High-resolution bathymetry data were collected within the deployment site for the RITE project (see Fig. 4(c)) in 2015 on a grid of  $0.15\text{ m} \times 0.15\text{ m}$ . Using this bathymetry survey, a digital elevation model of the river was created by discretizing the river bed with an unstructured triangular mesh with approximately  $2.2 \times 10^5$  triangular elements and  $4.4 \times 10^5$  points. Some regions within the river, where survey data was missing, were truncated and/or interpolated to provide the bathymetry immersed boundary. The digital elevation model for the 675 *m* long simulated reach is shown in Fig 5(a). The width of the channel in this reach varies between 175 *m* and 220 *m* while the flow depth varies between 2 *m* and 13 *m* with most common depth over the reach being approximately 10 *m*. Depths are relative to NAVD 88 datum.

### 5 East River Simulation Without Turbines

In this section we report the results of LES of the turbulent flow in the East River reach without the turbines at the nominal inflow value. This baseline simulation will provide the baseline of the river flow to subsequently investigate the effect of installing the array of turbines in the river. The simulation results are also compared with limited field measurements in terms of a single vertical velocity profile measured using Acoustic Doppler Current Profiler (ADCP).



Figure 4: Perspective view of the New York City area: (a) North-northeast (NNE) panoramic view of Manhattan; (b) West-southwest (WSW) view of the East River and showing the location of the field-scale study of marine hydrokinetic turbine array, map data ©2017 Google. (c) RITE project boundaries with proposed TriFrame locations ( $\Delta$ ). Copyright of Verdant Power Inc. (Verdant Power, 2010).



### 5.1 Computational setup

A Cartesian box of size  $720\text{ m}$ ,  $14\text{ m}$  and  $270\text{ m}$  in the streamwise (Z), spanwise (X) and vertical (Y) directions, respectively, was chosen as the computational domain within which the digitally reconstructed river bathymetry is immersed (see Fig. 5). The shore-line for the river was extracted using the ArcGIS mapping tool from a satellite map made available within the tool. This ensured that the physical shore-lines of the river are accurately captured in the computational domain. The bathymetry was then extended outside of the river boundaries to span the computational domain in the XZ plane (see Fig. 5(b)). Finite positive depth ( $1\text{ m}$ ) was assigned to on-shore region in the land. The outlet boundary section was artificially extended by repeating the last bathymetry cross section over  $100\text{ m}$  in the streamwise direction. This artificially created straight section of the river is used to facilitate application of outflow boundary conditions and eliminate spurious reflections at the downstream boundary that could contaminate the simulated flow and destabilize the flow solver.

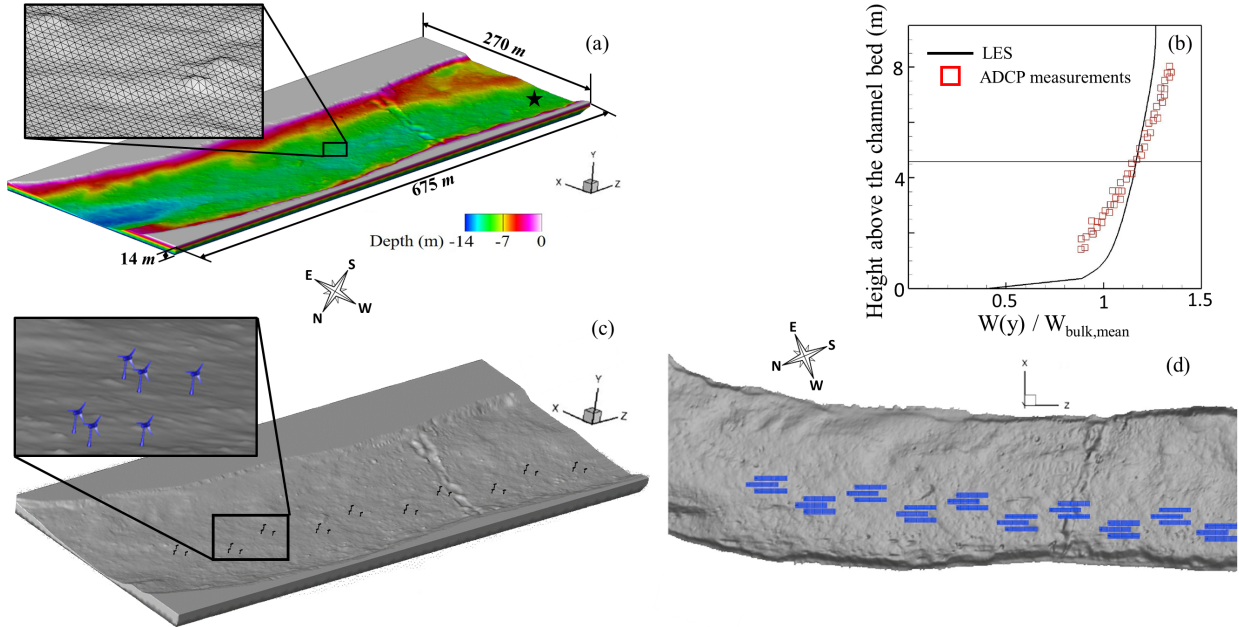


Figure 5: Computational domain and digital elevation model of simulated channel. A sample channel bathymetry is shown in the inset window represented by unstructured mesh. A star in (a) marks the location where an Acoustic Doppler Current Profiler (ADCP) was placed for measurement in the field. (b) Comparison of computed and measured velocity in the East River. Horizontal solid line denotes hub-height position if a turbine were to be placed here. (c) East River model with array of 30 turbines in TriFrame arrangement and (d) local grid refinement in the wake of each turbine.

Fig. 5(a) shows a sample of the unstructured triangular mesh which has been generated to discretize the river's bed topography, as needed by the sharp interface immersed boundary method in VFS-Rivers. The bottom bed was treated as a rigid bed with no sediment transport since it is made of large rocks on bedrock. A wall modeling approach, as described earlier, was used for the boundary condition on the bed. At the inlet boundary of the domain, instantaneous flowfields from a pre-computed fully developed turbulent flow are prescribed so that statistically the inflow corresponds to fully developed turbulent flow through a straight channel with cross-section identical to the most upstream cross-section of the East River bathymetry used in the simulations. That is, the so prescribed flowfields were obtained from a precursory LES through a straight channel with periodic boundary conditions in the streamwise direction. Naturally, the so prescribed inflow conditions do not correspond to the actual state of the river flow at the entrance of the East River reach we simulate herein. However, we note here that for the turbine simulations presented next, the streamwise distance between the inflow section and the most upstream turbine in the array is  $12D$  allowing for sufficient distance for the flow to develop over the actual river bathymetry before it encounters the turbines. At the downstream outlet boundary of the domain, Neumann (zero streamwise gradient) boundary conditions were imposed for all three velocity components. The river free surface is treated as rigid lid.

The nominal flow rate in the river and representative velocity based on the ADCP-measurements by Verdant Power were approximated to be  $3.28 \times 10^3 \text{ m}^3/\text{s}$  with a  $2 \text{ m}/\text{s}$ , respectively. From the bathymetry survey, the modal depth in the channel is approximately  $H = 10 \text{ m}$ . Using the above values of velocity and depth, the Reynolds number in the river is  $2 \times 10^7$ , which is typical value for river flows. The background Cartesian domain was discretized with  $360 \times 40 \times 1036$  cells in the X, Y and Z directions, respectively, i.e. a total of  $1.49 \times 10^7$  grid cells. Grid points are distributed uniformly in all three directions, resulting in spacing of  $0.75 \text{ m}$ ,  $0.35 \text{ m}$  and  $0.7 \text{ m}$  in the X, Y and Z directions, respectively. The time step in the calculations corresponds to Courant-Friedrichs-Lewy (CFL) number of  $CFL = 0.03$ . The simulations were carried out until the total kinetic energy in the domain is statistically converged. Subsequently, the flow-field was averaged for approximately 3 flow-through times where a flow-through time is defined as time taken to travel the streamwise extent of the domain at velocity  $W_b$ , which is the bulk inlet velocity. The simulations were performed on 264 processors of HPC clusters composed of Intel 2.4 GHz processors for approximately 1 month.

## 5.2 Comparisons with field measurements

A single velocity profile was measured in the river using ADCP along the depth at the Universal Transverse Mercator (UTM) coordinates of (588987.03 E, 4513118.35 N) in zone 18N, hereafter known as ADCP-N location also shown in Fig. 5(a). Figure 5(b) shows comparison of computed mean velocity with the field measurements in the East River provided by Verdant Power. Any discrepancies between the experimental measurements and the numerical calculations could be attributed to the following. The river bathymetry used in this simulation was obtained in 2015 whereas the ADCP velocity measurements at the above-mentioned location were obtained nearly 2 years earlier. This time difference naturally resulted in discrepancies in the exact bathymetry in the vicinity of ADCP-N location due to natural evolution of the river bed thereby altering the flowfield. The reported flow-depth from the measurements was  $9.16 \text{ m}$  approximately 10 % less than  $9.82 \text{ m}$  observed during the 2015 survey. Moreover, the exact flow-rate of the river at the time of the measurements was unknown and it was only approximated using the point measurement and assuming same mean velocity across a cross-section approximately perpendicular to the nominal flow direction in the channel. Due to the nature of the site, it is extremely difficult to obtain high fidelity field measurements and turbulence statistics that are accurately correlated with the time of tide in the East Channel. Hence, in the limit of available data and considering the variability of the processes involved, we argue that the simulations are in general agreement with the measurements. The average relative error is around 6%, which is acceptable considering the complexity of the calculation and the uncertainties mentioned above. We also point to the extensive validation studies of the VFS-Rivers code for flows in rivers and streams and for cases for which detailed mean flow and turbulence statistics measurements were available (Kang et al., 2011; Khosronejad et al., 2016a), which build confidence in the accuracy of the present simulations. More results for this case are shown in next section in comparison with the turbine array simulation.

## 6 Simulation of East River with the turbine array

In this section, we carry out and discuss the results of LES of 10 TriFrames of axial hydrokinetic turbines installed on the river bed per the array design developed by Verdant Power is performed. Using the Verdant Power's Generation 5 Free Flow System axial hydrokinetic turbines (Colby and Corren, 2018), the 30 turbine array is placed in the East River section as shown in Fig. 5(c). The turbine rotors are  $5 \text{ m}$  in diameter and the hub height is  $4.58 \text{ m}$  from the bottom. This height is fixed due to the construction of the TriFrame and is uniform for all turbines. The distance between the turbine's hub from the free surface is variable depending on the depth of the channel at the individual turbine installation location. The geometrical details of the TriFrames as well as their hydrodynamic efficiency and wake characteristics have been the subject of a recently published paper by Chawdhary et al. (2017). The TriFrames from first to last, in the positive Z direction, are numbered as TF-10 to TF-1 in reverse order in the Verdant's proposed location.

The computational grid for this simulation is derived from the one used for the baseline case in the previous section. Two-level geometry-based adaptive mesh refinement was applied to the baseline grid to obtain high resolution in the wake region of the turbines. The local refinement was along an elliptical cylinder with the central axis of the cylinder aligned with the center of the turbines. For each turbine, the extent of the refinement region is  $1.4D$  and  $2D$  in vertical and spanwise directions, respectively. The refinement region further extends from  $1D$  upstream of turbine location to  $7D$  downstream of the turbine. The grid refinement procedure added approximately  $9.4 \times 10^6$  cells, resulting in the post-refinement grid having  $2.43 \times 10^7$  number of Cartesian cells. The grid cells were Cartesian and aspect ratio was 2.1:1:2 for all the cells in X, Y and Z directions, respectively. The local resolution in the turbine wake was  $0.1875 \text{ m}$ ,  $0.0875 \text{ m}$ ,  $0.1872 \text{ m}$  in the X, Y and Z directions, respectively, which corresponds to 27, 57, 29 points per turbine diameter. Such a grid resolution is known to give acceptable results for the turbine modeled with an actuator line model (Yang et al., 2013a). Actuator line models have been previously used successfully to predict the far wake dynamics of axial hydrokinetic turbines (Kang et al., 2014; Churchfield et al., 2013) and wind turbines (Yang et al., 2013b; Porté-Agel et al., 2013; Angelidis et al., 2016). Also, it is evident from prior numerical studies (Angelidis et al.,

2016) and the results we present herein that the proposed numerical framework allows turbine simulations on locally refined grids without introducing any artificial reflection of the vortical structures at the coarse/fine interface of the computational mesh.

The rest of the flow and boundary conditions were the same as used for the baseline flow simulation in the Section 5.1. The simulation was run until the total kinetic energy in the domain is statistically converged which happened in approximately 1.2 flow-through times to obtain turbulent statistics. The flow-field was then averaged for another 5 flow-through times.

### 6.1 Results

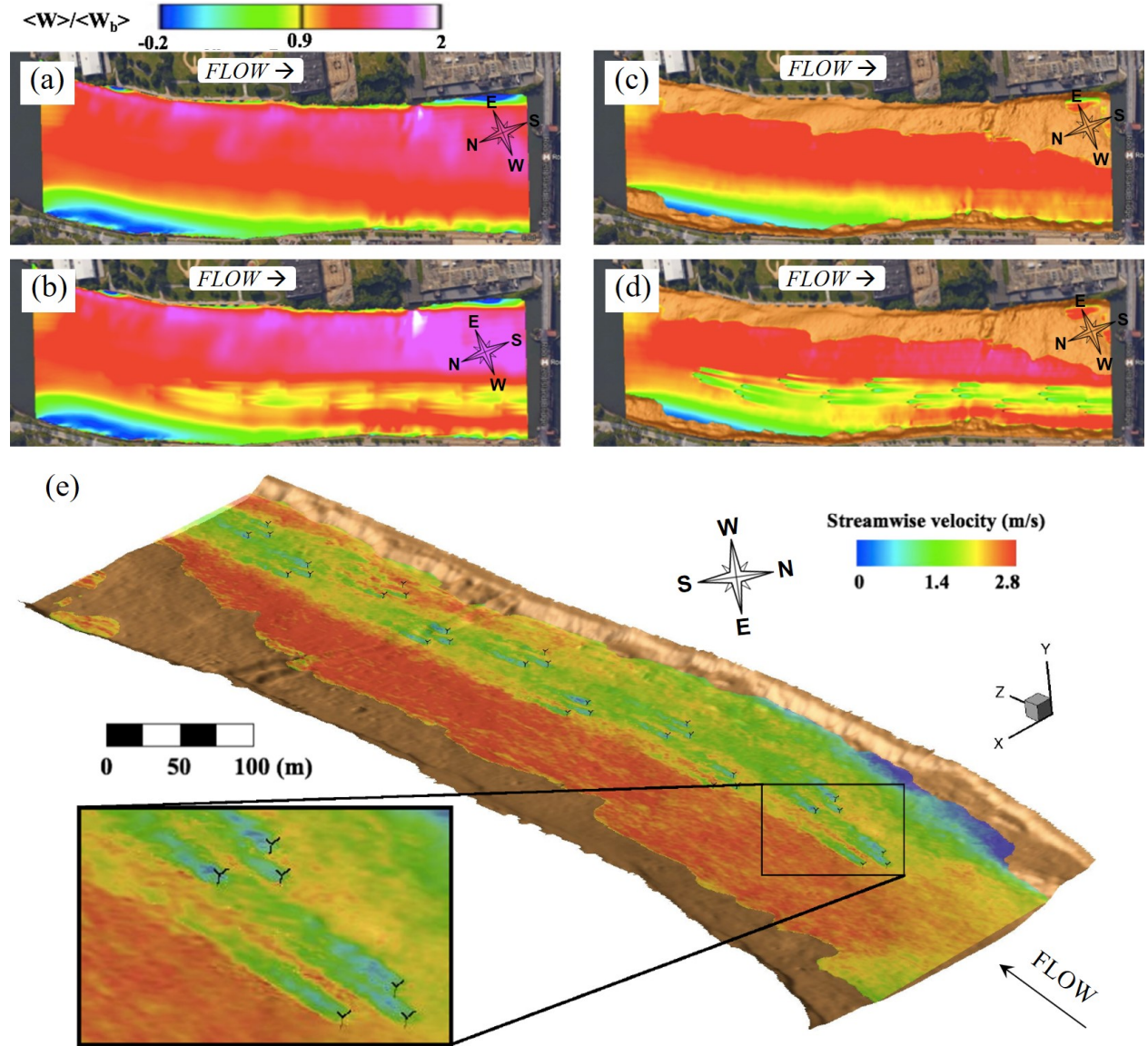


Figure 6: Contours of time-averaged streamwise velocity of the East Channel of East River, normalized by the bulk mean inflow velocity, in an XZ plane at free surface (a) without turbines, (b) with turbines, and at 7 m depth (c) without turbines, (d) with turbines. (e) Contours of instantaneous streamwise velocity in an XZ plane 7 m below the free surface with TriFrames.

Figure 6(a) and (b) shows the contours of time-averaged streamwise velocity at the freesurface of the channel. The results from the baseline simulation without turbines are also shown using the same contour levels for comparison. The baseline simulation shows that the velocity at the freesurface is higher in the upper half South-East side of the river.

The kink in the geometry North-East of the East River, which is essentially upstream of the simulated section of the channel, is responsible for the generation of a significant wake region in the flow. Hence, the velocity distribution is greatly affected by the strong deceleration in northwest of the east channel of the East River. Its effect on the simulated section is caused because of the precursory simulation for generating the inflow. The domain for inflow generation was generated by extrusion in the streamwise ( $Z$ ) direction. This is a reasonable approximation because the channel upstream of the inflow section is straight at the end of curvature. As we already discussed, this was necessitated because bathymetric data was available only for a limited channel reach. Ideally, the simulated channel reach should extend upstream of the present channel and VFS-Rivers is capable of handling such an extended domain. However, realizing this requires more detailed bathymetry data and is beyond the scope of the present work. The contours from the simulation with the turbine array installed show a similar trend as the baseline case with high velocity in the upper half of the river. There is a weak signature of the turbine wakes marked by the region of reduced velocity on the free-surface of the channel. The footprint of the turbine wake on the surface flow is more pronounced for the TriFrames in the middle of the array. The first two TriFrames barely show any effect on the free surface. This is because the hub height of these turbines is much lower compared to the other TriFrames – this is evident from the digital elevation model showing depth contour in the river (Fig. 5(a)).

In Fig. 6(c) and (d), the contours of time-averaged velocity are shown on a horizontal plane  $7\text{ m}$  below the free surface. The hub of the upstream turbines is located approximately  $7\text{ m}$  below the free surface. In Fig. 6(c), we note for the baseline simulation a distinct feature of the bathymetry on the bottom-left corner where a ridge is seen to contribute to the slow velocity wake in this region discussed earlier. In Fig. 6(d), the wakes of the turbines are clearly visible. The wakes of the first three TriFrames, specifically the first and second, do not align with the axis of rotation. This indicates that the yawing mechanism of the turbines should turn them in the primary incoming flow direction which, for these turbines, is not in  $Z$  directions. The yawing mechanism was not modeled in the present case (instead the turbines were assumed fixed in direction), hence we see the wake alignment departing from the axis of rotation. The overall wake of the array suggests that the staggering of the 10 TriFrames as proposed by Verdant Power is more efficient for energy extraction because of higher incoming flow momentum for the downstream TriFrames. Additionally, Fig. 6(e) shows contours of instantaneous streamwise velocity on a plane  $7\text{ m}$  below the free surface, i.e. near the hub-height of the first TriFrame. This contour plot clearly shows the complex dynamics of the flow captured in the simulation. The large range of the scales present in the model can be readily seen. The  $5\text{ m}$ -diameter turbine is orders of magnitudes smaller than the dimensions of the river. Yet, the unstructured Cartesian grid enabled us to locally refine the grid and resolve the flow in the wake of turbines. The complex interaction of the scales resolved by the refined grid is shown in the inset figure for a smaller highlighted region. An equivalent uniform structured grid, with resolution equal to the maximum achieved in the wake of the turbines, would consist of a staggering  $9.5 \times 10^8$  cells (close to one billion); making such a “brute-force” calculation extremely demanding from the computational standpoint. Being able to carry out LES across such a broad range of spatial scales using relatively coarse grids (compared to those that would be required for “brute-force” simulations) is only possible using the proposed multi-resolution modeling framework with local refinement.

Figure 7(a) shows contours of time-averaged vorticity magnitude at the free surface of the river without the turbine array. There is no significant vorticity at the free surface for the scale shown here, except for the vorticity generated by the river banks. For the simulation with the turbine array, Fig. 7(b) shows that the TriFrames make only a weak mark on free surface vorticity values. In fact their surface signature is only visible using the exaggerated scales selected for this purpose in Fig. 7(b). In Fig. 7(c) and (d), the time-averaged vorticity contours are shown at the  $XZ$  planes  $5\text{ m}$  and  $7\text{ m}$  below the free surface of the channel, respectively. The wakes of the turbines show higher vorticity magnitude, which was absent when no turbines were installed. The vorticity magnitude contours follow the low velocity wakes similar to the streamwise vorticity distribution. Higher vorticity also exists near the banks and other geometrical features of the river bed as seen in Fig. 7(c) near the downstream end of the channel.

## 6.2 How TriFrames affect the flow in East River

The presence of the turbine array alters the flow patterns in the river by extracting momentum from the stream flow and increasing the turbulence kinetic energy (TKE). In Fig. 8 we compare the calculated mean streamwise velocity profiles at several downstream location in the river, approximately halfway between the TriFrames. In the first plot 8(a), the velocity 6D upstream of the first TriFrame is the same for the baseline as well as flow with the turbines. A possible reason for this could be the effect of not accounting for the blockage effect the turbines would impart on the large-scale East River flow whereby the flow could bypass to the west channel of the East River if a larger region was considered in the simulation. However, we stipulate that given the small blockage ratio of a TriFrame (0.033%) the bypass flow to the West Channel of the East River would not be significant (Chen and Liou, 2011; Nishino and Willden, 2012a) – the validity of this assertion, however, remains to be confirmed by future simulations considering a much large section of the East River with the Roosevelt Island included in the model. In the next plot Fig. 8(b), 6D downstream of the

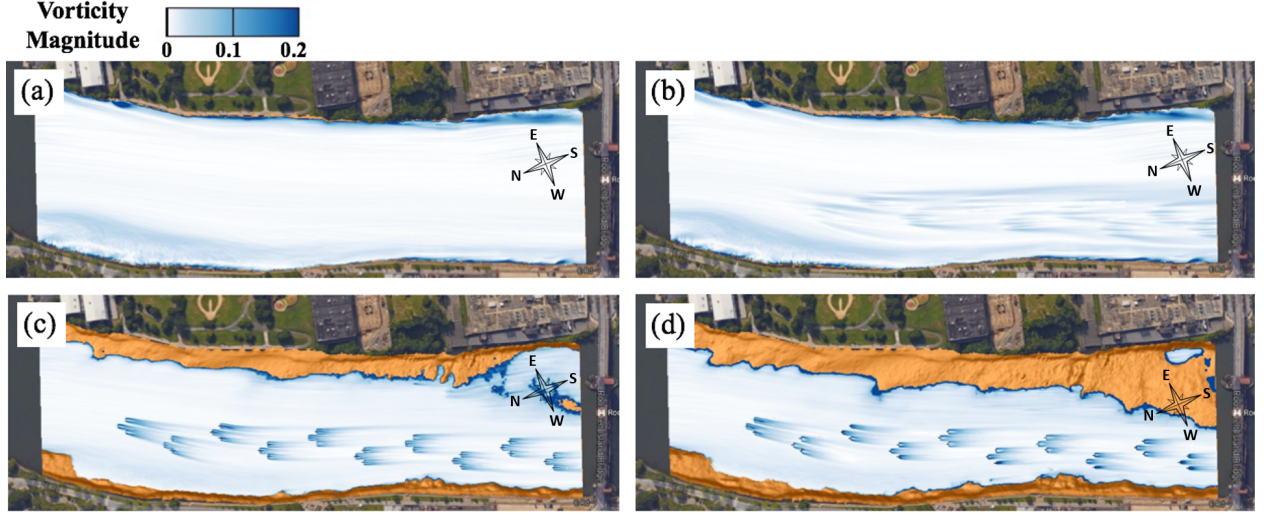


Figure 7: Contours of time-averaged vorticity magnitude normalized by the bulk mean inflow velocity  $W_b/D$  and rotor diameter  $D$  in an XZ plane of East River (a) without turbine array at free surface, and with 10 TriFrames of turbines installed at (b) free surface, (c) 5 m depth and (d) 7 m depth.

first TriFrame, flow de-acceleration is observed in the spanwise location of the turbines. The W-shaped profile marks the signature of the two downstream turbines of the TriFrame. This shape is similar to the TriFrame wake signature from a single wake TriFrame study. The profile in Fig. 8(c) appears to be more similar to the TriFrame wake signature since the hub of second TriFrame is closer to 5 m depth. Similar wake signature is seen for the following TriFrames. In Fig. 8(d) through 8(k), the presence of turbines result in higher flow velocity in the bypass region around the turbines. Noticeably, the span where there was no turbine shows only slightly (up to 10% in 8(i)) higher streamwise velocity.

Fig. 9 shows transverse profiles of the TKE at the same locations as in Fig. 8 with and without the turbine array installed. As expected, the incoming flow upstream of the array shows relatively higher levels of TKE generated by the river banks. This is consistent with the incoming flow fed as the inflow boundary condition which was generated by assuming a straight channel extending upstream of the river with the same cross-section as the inlet section. The remaining profiles in Fig. 9 (b through k) reveal higher levels of TKE in the wake of every TriFrame, which is the expected effect of TriFrame added turbulence in the baseline river flow. It is worth noting, however, that the effect of the TriFrames is restricted in the immediate vicinity of the turbines as the levels of turbulence near the left (relative to the turbines as shown in Fig. 8) bank are almost identical with and without turbines.

## 7 Conclusions

In this work we demonstrated the use of a powerful numerical framework to successfully perform a LES at site-scale of a natural marine environment with a MHK turbine array. Such numerical undertaking was possible with the use of high performance computing and the new generation of the VFS-Rivers code featuring local mesh refinement on unstructured Cartesian grids. Locally refined grids allowed the bridging of scales between the river channel and the turbines and the wakes they induce on a grid with significantly smaller (by two orders of magnitude) number of grid nodes than that would be required using a “brute-force” approach—i.e. discretizing the entire river channel with a uniform grid with spacing small enough to resolve the wake of each turbine. More specifically, we were able to perform simulations on a grid with 24 million grid nodes with local resolution near the turbines ranging from  $D/27$  to  $D/57$ . Similar resolution with the brute-force approach would require close to one billion grid nodes. Simulations were first performed in the river for a nominal flow rate without the turbines to obtain baseline flow characteristics. Field measurements in the river were made using an ADCP to obtain a vertical profile of streamwise velocity at a single location. The velocity profile from the baseline flow was compared with this available velocity profile. The prediction of velocity profile showed reasonable agreement with the field data but also underscored the difficulties in obtaining measurements of sufficient quality in harsh tidal environments to enable detailed validation of computational methods at field scale. Future work in this site should focus on obtaining simultaneous measurements of river bathymetry and flow statistics at several locations through the channel to enable a more comprehensive validation of the flow solver for the baseline case.

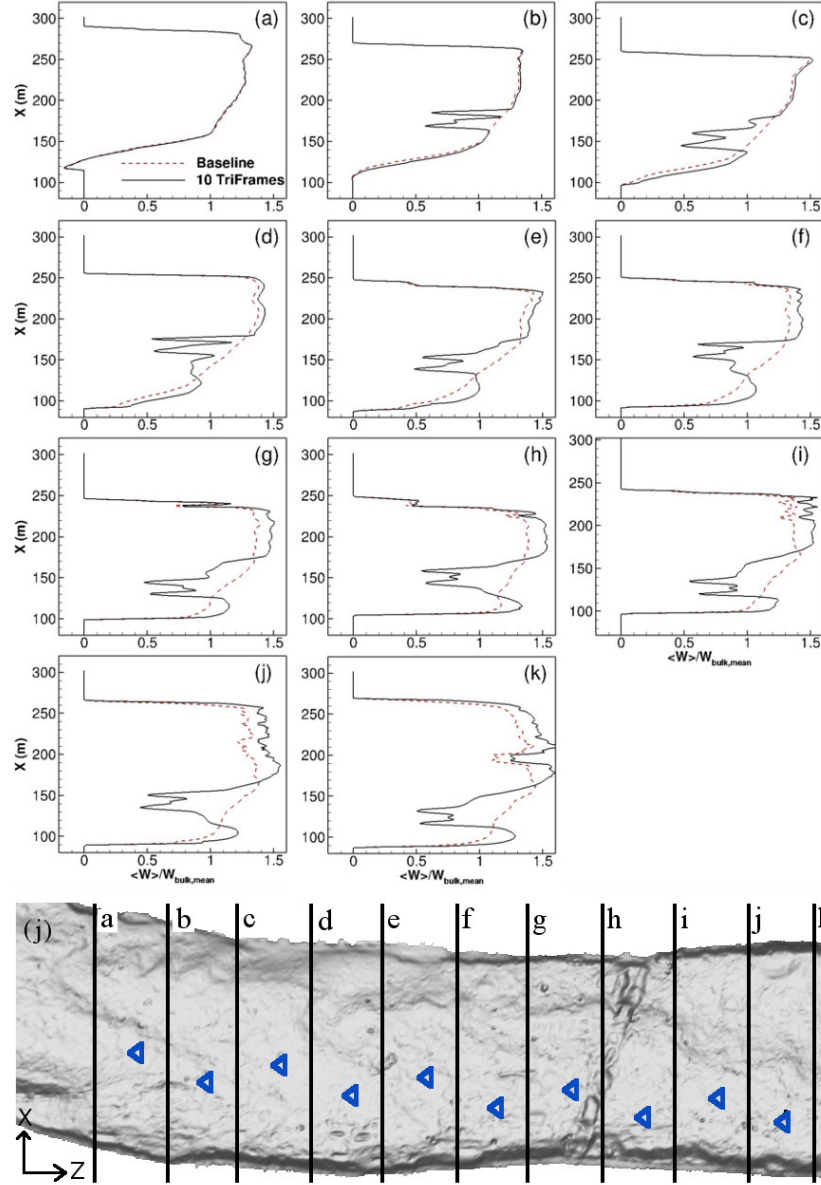


Figure 8: Transverse profiles of streamwise velocity on the  $XZ$  plane 5 m below the free surface of the East River along spanwise ( $X$ ) direction with and without 10 TriFrames of turbines installed at locations (a)  $Z = -23.8 m$  (b)  $Z = 36.2 m$  (c)  $Z = 93.6 m$  (d)  $Z = 154.4 m$  (e)  $Z = 213.2 m$  (f)  $Z = 274.5 m$  (g)  $Z = 332.7 m$  (h)  $Z = 393.9 m$  (i)  $Z = 454.1 m$  (j)  $Z = 515.2 m$  (k)  $Z = 569.3 m$ . Location (a) is 6D upstream of first TriFrame and following locations are 6D downstream of successive TriFrames. (l) shows the lines along which profiles were extracted.

LES of the East River channel with the 30 turbine array in place, arranged in 10 TriFrames, provided valuable insights about the hydrodynamics of the array and its impact on the baseline river flow. The bathymetry of the river site resulted in distinct site-specific flow patterns that can only be simulated by data-informed simulations such as those we reported herein. Our simulations indicated a marginal acceleration on the baseline river flow in the regions where turbines were not present. Comparison with the baseline flow in terms of mean streamwise velocity as well as vorticity magnitude indicates that there is a very small signature of the turbine wake at the free surface of the channel, thus, suggesting that the array would have essentially no effect on the navigability of the East River while it operates. Overall, the surface effects of the array are found to be negligible compared to the free surface disturbances already present in the baseline flow of tidal channel. The wakes of the first few TriFrames of the array were not aligned with the axis of rotation

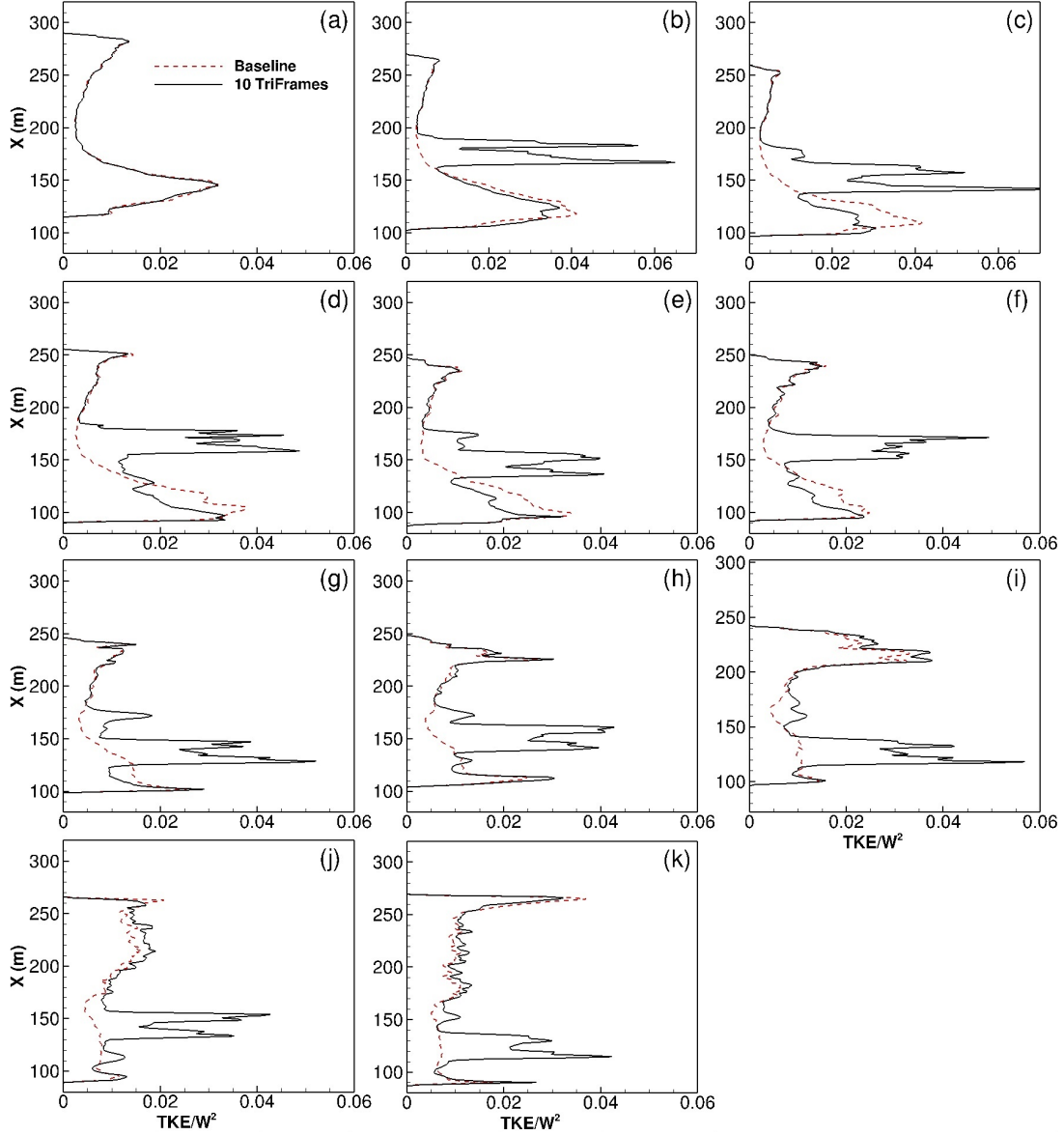


Figure 9: Turbulent kinetic energy (TKE) profiles in XZ plane 5 m below the free surface of the East River along spanwise (X) direction with and without 10 TriFrames of turbines installed at locations (a)  $Z = -23.8\text{ m}$  (b)  $Z = 36.2\text{ m}$  (c)  $Z = 93.6\text{ m}$  (d)  $Z = 154.4\text{ m}$  (e)  $Z = 213.2\text{ m}$  (f)  $Z = 274.5\text{ m}$  (g)  $Z = 332.7\text{ m}$  (h)  $Z = 393.9\text{ m}$  (i)  $Z = 454.1\text{ m}$  (j)  $Z = 515.2\text{ m}$  (k)  $Z = 569.3\text{ m}$ . Location (a) is 6D upstream of first TriFrame and following locations are 6D downstream of successive TriFrames. Fig.8 (l) shows the lines along which profiles were extracted.

defined by orientation of turbines. This means that the yaw of the turbines should turn the turbine in the direction of the incoming flow. The yaw mechanism of the turbine was not modeled in the present simulation.

Future work will focus on refining the model to eliminate uncertainties so that we can obtain better answers regarding the site specific performance of the proposed array and the deployment site. In this study, for instance, only limited bathymetry data was available upstream of the turbine array. A more extensive bathymetry of the site is needed in order to avoid the unwanted effects created by the inflow boundary treatment due to the missing upstream section. Geometry-based adaptive grid refinement was adopted in the present simulations. However, in the future, temporal adaptive mesh refinement may also be adopted in the simulations, similar to many astronomical simulations (Iapichino et al., 2008; Fryxell et al., 2000). Coupled with efficient repartitioning algorithms, such simulations will enable dynamic resolution of coherent structures in the wake of the turbines while optimizing the computational efficiency. Such

capability will be especially useful when the yaw mechanism of the turbines will be include din the simulations to enable dynamic wake stirring.

## 8 Acknowledgement\*

This work was supported by National Science Foundation (NSF) grant number *IIP-1318201*. The bathymetry survey for the simulated section was provided by Verdant Power Inc. through a contractor Ocean Survey Inc. Computational resources were provided by the Minnesota Supercomputing Institute (MSI) at University of Minnesota.

## References

- Abad, J. D., Rhoads, B. L., Güneralp, İ., and García, M. H. (2008). Flow structure at different stages in a meander-bend with bendway weirs. *Journal of Hydraulic Engineering*, 134(8):1052–1063.
- Abderrezzak, K. E. K., Paquier, A., and Mignot, E. (2009). Modelling flash flood propagation in urban areas using a two-dimensional numerical model. *Natural Hazards*, 50(3):433–460.
- Abolghasemi, M. A., Piggott, M. D., Spinneken, J., Viré, A., Cotter, C. J., and Crammond, S. (2016). Simulating tidal turbines with multi-scale mesh optimisation techniques. *Journal of Fluids and Structures*, 66:69–90.
- Adcock, T. A., Draper, S., and Nishino, T. (2015). Tidal power generation—a review of hydrodynamic modelling. *Proceedings of the Institution of Mechanical Engineers, Part A: Journal of Power and Energy*, 229(7):755–771.
- Angelidis, D., Chawdhary, S., and Sotiropoulos, F. (2016). Unstructured cartesian refinement with sharp interface immersed boundary method for 3D unsteady incompressible flows. *Journal of Computational Physics*, 325:272–300.
- Angeloudis, A., Kramer, S. C., Avdis, A., and Piggott, M. D. (2018). Optimising tidal range power plant operation. *Applied Energy*, 212:680–690.
- Bai, L., Spence, R. R., and Dudziak, G. (2009). Investigation of the influence of array arrangement and spacing on tidal energy converter (TEC) performance using a 3-dimensional CFD model. In *Proceedings of the 8th European Wave and Tidal Energy Conference, Uppsala, Sweden*, pages 654–660.
- Balay, S., Abhyankar, S., Adams, M. F., Brown, J., Brune, P., Buschelman, K., Dalcin, L., Eijkhout, V., Gropp, W. D., Kaushik, D., Knepley, M. G., McInnes, L. C., Rupp, K., Smith, B. F., Zampini, S., Zhang, H., and Zhang, H. (2016). PETSc users manual. Technical Report ANL-95/11 - Revision 3.7, Argonne National Laboratory.
- Balay, S., Abhyankar, S., Adams, M. F., Brown, J., Brune, P., Buschelman, K., Eijkhout, V., Gropp, W. D., Kaushik, D., Knepley, M. G., McInnes, L. C., Rupp, K., Smith, B. F., and Zhang, H. (2014). PETSc Web page.
- Balay, S., Gropp, W. D., McInnes, L. C., and Smith, B. F. (1997). Efficient management of parallelism in object oriented numerical software libraries. In Arge, E., Bruaset, A. M., and Langtangen, H. P., editors, *Modern Software Tools in Scientific Computing*, pages 163–202. Birkhäuser Press.
- Baranya, S., Olsen, N., and Józsa, J. (2015). Flow analysis of a river confluence with field measurements and rans model with nested grid approach. *River research and applications*, 31(1):28–41.
- Batten, W., Bahaj, A., Molland, A., and Chaplin, J. (2008). The prediction of the hydrodynamic performance of marine current turbines. *Renewable Energy*, 33(5):1085–1096.
- Calderer, A., Yang, X., Angelidis, D., Khosronejad, A., Le, T., Kang, S., Gilmanov, A., Ge, L., and Borazjani, I. (2015). Virtual flow simulator, <http://www.osti.gov/scitech/servlets/purl/1312901>.
- Casulli, V. and Walters, R. A. (2000). An unstructured grid, three-dimensional model based on the shallow water equations. *International Journal for Numerical Methods in Fluids*, 32(3):331–348.
- Chamorro, L. P. and Porte-Agel, F. (2011). Turbulent flow inside and above a wind farm: a wind-tunnel study. *Energies*, 4(11):1916–1936.
- Chamorro, L. P., Troolin, D. R., Lee, S.-J., Arndt, R., and Sotiropoulos, F. (2013). Three-dimensional flow visualization in the wake of a miniature axial-flow hydrokinetic turbine. *Experiments in fluids*, 54(2):1459.



- Chawdhary, S., Hill, C., Yang, X., Guala, M., Corren, D., Colby, J., and Sotiropoulos, F. (2017). Wake characteristics of a triframe of axial-flow hydrokinetic turbines. *Renewable Energy*, 109:332–345.
- Chen, T. and Liou, L. (2011). Blockage corrections in wind tunnel tests of small horizontal-axis wind turbines. *Experimental Thermal and Fluid Science*, 35(3):565–569.
- Churchfield, M., Lee, S., Moriarty, P., Martinez, L., Leonardi, S., Vijayakumar, G., and Brasseur, J. (2012). A large-eddy simulation of wind-plant aerodynamics. In *50th AIAA Aerospace Sciences Meeting including the New Horizons Forum and Aerospace Exposition*, page 537.
- Churchfield, M. J., Li, Y., and Moriarty, P. J. (2013). A large-eddy simulation study of wake propagation and power production in an array of tidal-current turbines. *Philosophical Transactions of the Royal Society A: Mathematical, Physical and Engineering Sciences*, 371(1985):20120421.
- Colby, J. and Corren, D. (2018). Free flow system technology by verdant power.
- Falgout, R. D., Jones, J. E., and Yang, U. M. (2006). *The Design and Implementation of hypre, a Library of Parallel High Performance Preconditioners*, pages 267–294. Springer Berlin Heidelberg, Berlin, Heidelberg.
- Fryxell, B., Olson, K., Ricker, P., Timmes, F., Zingale, M., Lamb, D., MacNeice, P., Rosner, R., Truran, J., and Tufo, H. (2000). Flash: An adaptive mesh hydrodynamics code for modeling astrophysical thermonuclear flashes. *The Astrophysical Journal Supplement Series*, 131(1):273.
- Gant, S. and Stallard, T. (2008). Modelling a tidal turbine in unsteady flow. In *Proceedings of the Eighteenth (2008) International Offshore and Polar Engineering Conference*, pages 473–480.
- Ge, L. and Sotiropoulos, F. (2005). 3d unsteady rans modeling of complex hydraulic engineering flows. i: Numerical model. *Journal of Hydraulic Engineering*, 131(9):800–808.
- Ge, L. and Sotiropoulos, F. (2007a). A numerical method for solving the 3D unsteady incompressible navier-stokes equations in curvilinear domains with complex immersed boundaries. *Journal of computational physics*, 225(2):1782–1809.
- Ge, L. and Sotiropoulos, F. (2007b). A numerical method for solving the 3D unsteady incompressible navier-stokes equations in curvilinear domains with complex immersed boundaries. *Journal of Computational Physics*, 225(2):1782–1809.
- Hamrick, J. (2007). The environmental fluid dynamics code: theory and computation. *US EPA, Fairfax, VA*, pages 10–15.
- Heniche, M., Secretan, Y., Boudreau, P., and Leclerc, M. (2000). A two-dimensional finite element drying-wetting shallow water model for rivers and estuaries. *Advances in Water Resources*, 23(4):359–372.
- Iapichino, L., Adamek, J., Schmidt, W., and Niemeyer, J. (2008). Hydrodynamical adaptive mesh refinement simulations of turbulent flows–i. substructure in a wind. *Monthly Notices of the Royal Astronomical Society*, 388(3):1079–1088.
- James, S. C., Seetho, E., Jones, C., and Roberts, J. (2010). Simulating environmental changes due to marine hydrokinetic energy installations. In *OCEANS 2010*, pages 1–10. IEEE.
- Kang, S., Borazjani, I., Colby, J. A., and Sotiropoulos, F. (2012). Numerical simulation of 3D flow past a real-life marine hydrokinetic turbine. *Advances in Water Resources*, 39:33–43.
- Kang, S., Lightbody, A., Hill, C., and Sotiropoulos, F. (2011). High-resolution numerical simulation of turbulence in natural waterways. *Advances in Water Resources*, 34(1):98–113.
- Kang, S. and Sotiropoulos, F. (2012). Numerical modeling of 3D turbulent free surface flow in natural waterways. *Advances in Water Resources*, 40:23–36.
- Kang, S. and Sotiropoulos, F. (2015). Numerical study of flow dynamics around a stream restoration structure in a meandering channel. *Journal of Hydraulic Research*, 53(2):178–185.
- Kang, S., Yang, X., and Sotiropoulos, F. (2014). On the onset of wake meandering for an axial flow turbine in a turbulent open channel flow. *Journal of Fluid Mechanics*, 744:376–403.

- Khan, M., Bhuyan, G., Iqbal, M., and Quaicoe, J. (2009). Hydrokinetic energy conversion systems and assessment of horizontal and vertical axis turbines for river and tidal applications: A technology status review. *Applied Energy*, 86(10):1823–1835.
- Khosronejad, A., Hansen, A., Kozarek, J., Guentzel, K., Hondzo, M., Guala, M., Wilcock, P., Finlay, J., and Sotiropoulos, F. (2016a). Large eddy simulation of turbulence and solute transport in a forested headwater stream. *Journal of Geophysical Research: Earth Surface*, 121(1):146–167.
- Khosronejad, A., Le, T., DeWall, P., Bartelt, N., Woldeamlak, S., Yang, X., and Sotiropoulos, F. (2016b). High-fidelity numerical modeling of the upper mississippi river under extreme flood condition. *Advances in water resources*, 98:97–113.
- Lee, J., Lee, J., Yun, S.-L., and Oh, H.-C. (2017). Development of a finite volume two-dimensional model and its application in a bay with two inlets: Mobile bay, alabama. *Continental Shelf Research*, 146:13–27.
- Li, Y., Lence, B. J., and Calisal, S. M. (2011). An integrated model for estimating energy cost of a tidal current turbine farm. *Energy Conversion and Management*, 52(3):1677–1687.
- Lu, Y.-j. and Wang, Z.-y. (2009). 3d numerical simulation for water flows and sediment deposition in dam areas of the three gorges project. *Journal of hydraulic engineering*, 135(9):755–769.
- Malki, R., Masters, I., Williams, A. J., and Croft, T. N. (2014). Planning tidal stream turbine array layouts using a coupled blade element momentum–computational fluid dynamics model. *Renewable Energy*, 63:46–54.
- Musa, M., Hill, C., Sotiropoulos, F., and Guala, M. (2018). Performance and resilience of hydrokinetic turbine arrays under large migrating fluvial bedforms. *Nature Energy*, page 1.
- Nagata, N., Hosoda, T., Nakato, T., and Muramoto, Y. (2005). Three-dimensional numerical model for flow and bed deformation around river hydraulic structures. *Journal of Hydraulic Engineering*, 131(12):1074–1087.
- Nishino, T. and Willden, R. H. (2012a). Effects of 3-d channel blockage and turbulent wake mixing on the limit of power extraction by tidal turbines. *International Journal of Heat and Fluid Flow*, 37:123–135.
- Nishino, T. and Willden, R. H. (2012b). The efficiency of an array of tidal turbines partially blocking a wide channel. *Journal of Fluid Mechanics*, 708:596–606.
- OpenEI (2008). Early electrification of buffalo: 60-hz replaces 25-hz. [Online; accessed 05-August-2018].
- Porté-Agel, F., Wu, Y.-T., and Chen, C.-H. (2013). A numerical study of the effects of wind direction on turbine wakes and power losses in a large wind farm. *Energies*, 6(10):5297–5313.
- Saad, Y. and Schultz, M. H. (1986). GMRES: A generalized minimal residual algorithm for solving nonsymmetric linear systems. *SIAM Journal on Scientific and Statistical Computing*, 7(3):856–869.
- Smagorinsky, J. (1963). General circulation experiments with the primitive equations: I. the basic experiment. *Monthly Weather Review*, 91(3):99–164.
- Sotiropoulos, F. (2015). Hydraulics in the era of exponentially growing computing power. *Journal of Hydraulic Research*, 53(5):547–560.
- Stoesser, T., Ruether, N., and Olsen, N. R. B. (2010). Calculation of primary and secondary flow and boundary shear stresses in a meandering channel. *Advances in Water Resources*, 33(2):158–170.
- Tatum, S., Frost, C., Allmark, M., O’Doherty, D., Mason-Jones, A., Prickett, P., Grosvenor, R., Byrne, C., and O’Doherty, T. (2016). Wave–current interaction effects on tidal stream turbine performance and loading characteristics. *International Journal of Marine Energy*, 14:161–179.
- Torrens-Spence, H., Schmitt, P., Frost, C., Benson, I., Mackinnon, P., and Whittaker, T. (2017). Assessment of flow characteristics at two locations in an energetic tidal channel. In *European Wave & Tidal Energy Conference*.
- Vasel-Be-Hagh, A. and Archer, C. L. (2017). Wind farms with counter-rotating wind turbines. *Sustainable Energy Technologies and Assessments*, 24:19–30.
- Verdant Power, L. (2010). Pilot lisencc application roosevelt island tidal energy project FERC No. 12611. Technical Report 2, Verdant Power, LLC, Verdant Power, Inc., P.O. Box 282, Roosevelt Island, New York, NY 10044. Final kinetic hydropower pilot license application.

- Wang, M. and Moin, P. (2002). Dynamic wall modeling for large-eddy simulation of complex turbulent flows. *Physics of Fluids*, 14(7):2043–2051.
- Wilcox, K., Zhang, J., McLeod, I., Gerber, A., Jeans, T., McMillan, J., Hay, A., Karsten, R., and Culina, J. (2017). Simulation of device-scale unsteady turbulent flow in the fundy tidal region. *Ocean Engineering*, 145:59–76.
- Williamson, B. J., Blondel, P., Armstrong, E., Bell, P. S., Hall, C., Waggitt, J. J., and Scott, B. E. (2016). A self-contained subsea platform for acoustic monitoring of the environment around marine renewable energy devices—field deployments at wave and tidal energy sites in orkney, scotland. *IEEE Journal of Oceanic Engineering*, 41(1):67–81.
- Yang, U. M. and Henson, V. E. (2002). Boomeramg: a parallel algebraic multigrid solver and preconditioner. *Applied Numerical Mathematics*, 41(1):155–177.
- Yang, X., Kang, S., and Sotiropoulos, F. (2012). Computational study and modeling of turbine spacing effects in infinite aligned wind farms. *Physics of Fluids*, 24(11):115107.
- Yang, X., Kang, S., and Sotiropoulos, F. (2013a). Toward a simulation-based approach for optimizing mhc turbine arrays in natural waterways. In *Proceedings of the 1st Marine Energy Technology Symposium*.
- Yang, X., Pakula, M., and Sotiropoulos, F. (2018). Large-eddy simulation of a utility-scale wind farm in complex terrain. *Applied Energy*, 229:767–777.
- Yang, X., Sotiropoulos, F., Conzemius, R. J., Wachtler, J. N., and Strong, M. B. (2013b). Large-eddy simulation of turbulent flow past wind farms in complex terrains: The Virtual Wind Simulator (VWiS). *Wind Energy*, 16(1):1–20.
- Yang, X., Sotiropoulos, F., Conzemius, R. J., Wachtler, J. N., and Strong, M. B. (2015). Large-eddy simulation of turbulent flow past wind turbines/farms: the virtual wind simulator (VWiS). *Wind Energy*, 18(12):2025–2045.
- Yoon, T. H. and Kang, S.-K. (2004). Finite volume model for two-dimensional shallow water flows on unstructured grids. *Journal of Hydraulic Engineering*, 130(7):678–688.